

## Supporting Information

# Fabricating Carbon Quantum Dots with Nano-defined Position and Pattern in One Step via Sugar-Electron-beam-Writing

Yuyan Weng, Zhiyun Li, Lun Peng, Weidong Zhang, Gaojian Chen\*

Center for Soft Condensed Matter Physics and Interdisciplinary Research, Soochow University, Suzhou, 215006, China.

E-mail: gchen@suda.edu.cn

Tel: +86-512-65884406

## Instruments and characterization

The molecular weights and molecular weight distributions of PMAG were measured on an Agilent PL-GPC 50 equipped with a refractive index detector, using a 5 mm Guard, 5 mm MIXED-D column with PMMA standard samples and 0.05 mol L<sup>-1</sup> lithium bromide solution in DMF was used as the eluent at a flow rate of 1 mL min<sup>-1</sup> operating at 50°C. <sup>1</sup>H/<sup>13</sup>C NMR spectra of PMAG were recorded on an INOVA 300 MHz nuclear magnetic resonance (NMR) instrument, using D<sub>2</sub>O as the solvent. FT-IR spectra were recorded on a Nicolette-6700 FT-IR spectrometer. Energy dispersive x-ray analysis (EDAX) were recorded on an S-4700 SEM at a 15 kV accelerating voltage. X-ray photoelectron spectra (XPS) were recorded on an ESCALAB 250Xi (Thermo Scientific, USA) using Al K $\alpha$  X-rays in a standard mode. Ultraviolet-visible (UV-Vis) absorption spectra were performed on a Shimadzu (Kyoto, Japan) UV-3600. The confocal observation was measured on an inverted confocal laser scanning microscope (Zeiss, LSM 710). The fluorescence spectra was obtained under the dark field of the confocal system excited by 405 nm laser. In this circumstance, the Lambda mode was selected in the manual tools at the work interface (ZEN 2009) of the confocal laser scanning microscope. To improve the signal to noise ratio, the averaging number was chosen to be 8. And the wavelength resolution of the final luminescence spectrum is 3 nm. The super resolution microscopic images were obtained under the total internal reflection fluorescence (TIRF) mode of the super resolution optical microscope by Electron-Multiplying CCD (EMCCD, Andor, iXon 897U).

The atomic force microscope (AFM) experiments were performed using an Asylum Research M PF-3D scanning force microscope. The spring constant of cantilever in a tapping mode is ca. 3 N/m, and resonance frequency is 75 kHz. Static Water Contact Angle is measured on a SL200C optical contact angle meter (USA Kino Industry Co., Ltd) at room temperature. Thermal degradation of PMAG, PVA and Dextran was investigated by a Discovery TGA instrument (TA Instruments, USA) from room temperature to 800 °C with a heating rate of 10 °C/min under nitrogen atmosphere (50 ml/min).

## Materials

The initiator 2,2'-azobis(isobutyronitrile) (AIBN) (Shanghai Chemical Reagent Co. Ltd., China, 99%) was recrystallized three times from ethanol. 2-cyanoprop-2-yl-a-dithionaphthalate (CPDN) was synthesized and characterized according to a previously reported method.<sup>[S1]</sup> The two control polymers: poly(vinyl alcohol) (PVA, Mw = 31000) (Sigma-Aldrich), dextran (Mw = 10000) (Aladdin, China), All other chemicals and solvents were purchased from Sigma-Aldrich except for N-dimethylacetamide (DMAc) that were purchased from Sinopharm Chemical Reagent Co., Ltd.

## Synthesis of 2 - (methacrylamido) glucopyranose (MAG).

The monomers were prepared according to a previously reported work.<sup>[S2]</sup>

## Glycopolymer (PMAG) synthesis and characterization.



### Scheme S1 | Synthesis of PMAG via reversible addition-fragmentation (RAFT) polymerization.

The experimental procedure is schematically illustrated in Scheme S1. MAG (0.500 g, 2.0222 mmol), CPDN (0.0109 g, 0.0404 mmol), and AIBN (0.00169 g, 0.0101 mmol) N, N-

dimethylacetamide (DMAc, 2 mL) were added to a dry glass ampule with a magnetic bar. The above solution was purged with argon for 15 min to eliminate the oxygen. Then the ampule was flame-sealed and placed in an oil bath, held by a thermostat at 70°C. After 24 h, the ampule was cooled with ice water and opened. The reaction mixture was precipitated into an excess of methanol. The final polymer was dialyzed (membrane cut off of 3500 g mol<sup>-1</sup>) against distilled water for 2 days, and then freeze-dried for 3 days to obtain pink powder 0.32 g (64% conversion). GPC analysis (Fig. S2) gave a molecular weight of Mn = 9500 g mol<sup>-1</sup>, PDI = 1.14 (Mn(th) = 12300 g mol<sup>-1</sup>). <sup>1</sup>H NMR (300 MHz, D<sub>2</sub>O, ppm) (Fig. S1a): 7.3 – 8.1 (m, 7H, CH of naphthalene units), 5.0 – 5.35 (d, 1H, H-1 of galactose), 3.35 – 3.95 (m, 6H, H-2, H-3, H-4, H-5, H-6 of galactose), 1.7 – 1.8 (s, 2H, CH<sub>2</sub> of main chain), 0.8 – 1.0 (s, 3H, CH<sub>3</sub> of main chain). <sup>13</sup>C NMR (300 MHz, D<sub>2</sub>O, ppm) (Fig. S1b): a: 16.61 (C-10), b: 44.21 (C-8), c: 54.49 (C-9), d: 57.05 (C-2), e: 60.55 (C-6), f: 70.26 (C-3), g: 71.45 (C-4), h: 75.70 (C-5) i<sup>α</sup>: 90.02 (C-1<sub>α</sub>), i<sup>β</sup>: 94.58 (C-1<sub>β</sub>), j: 179.01 (C-7).

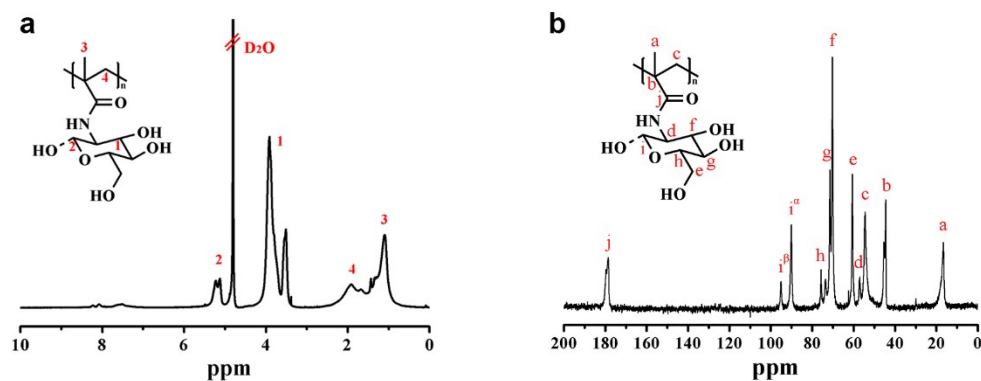


**Figure S1** | <sup>1</sup>H-NMR(a) and <sup>13</sup>C-NMR(b) (in D<sub>2</sub>O) spectrum of PMAG.

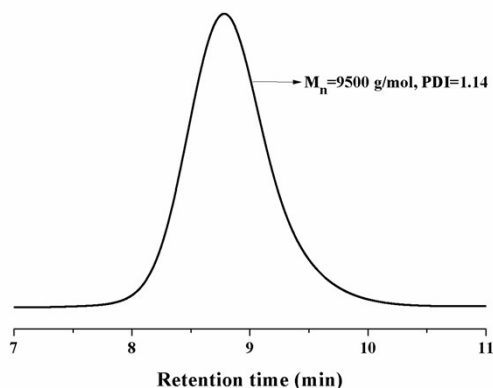


**Figure S2** | GPC spectrum (in DMF) of PMAG.

### **Characteristics of PMAG as a negative photoresist**

The spatial resolution of PMAG as a negative photoresist was shown in Fig. S3. Regular square arrays were fabricated on the ITO substrate by PMAG resist. The exposure dose value was chosen to be  $120 \mu\text{C}/\text{cm}^2$ . Under the treatment with  $1 \times 120 \mu\text{C}/\text{cm}^2$ , the PMAG film could only be cross-linked. And the designed squares could be presented by water development. With the dose factors increasing, the carbonization and aromatization would take place, and result in the fluorescent phenomenon. The histogram of the fluorescence intensity vs the dose factors was shown in Fig. 3e in the main text. The phase image and its enlarged image were shown in Fig. S3a-b. The profile image was also shown in Fig. S4 to exhibit the well-defined vertical profile at the edge of the single square. Figure S3c-f show the Scanning electron microscope (SEM) images of the samples with high-quality holes, lines, squares and meshes generated on PMAG films after electron beam exposure.

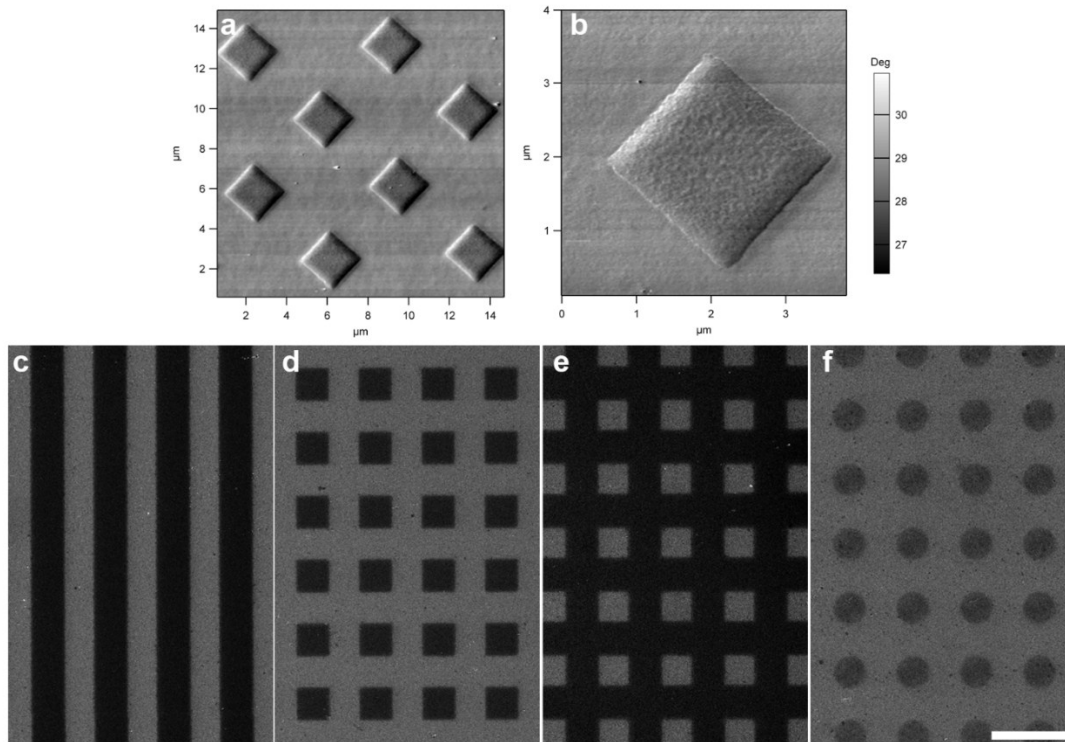


**Figure S3** | a-b, The square array of PMAG as negative photoresist; c-f, The PMAG patterns fabricated by EBL. The scale bars in f is 5  $\mu\text{m}$ .

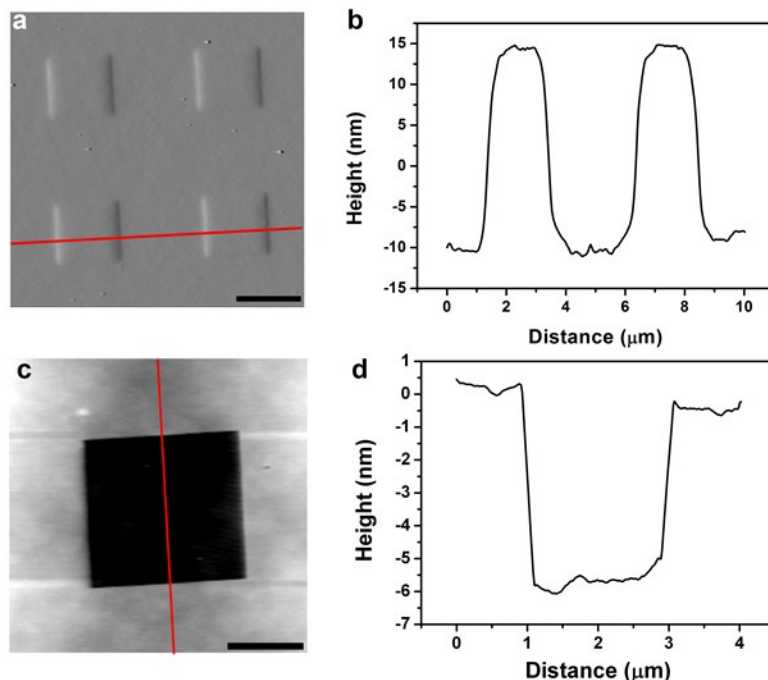


**Figure S4** | The profiles of the PMAG square array. a&b are PMAG with water developments; c&d are without water developments. The scale bars in a is 2  $\mu\text{m}$ , in c is 1  $\mu\text{m}$ .

### The comparison with the industrialized resist PMMA.

The PMAG resist worked as a negative photoresist. The electron exposure efficiency and the spatial resolution could be comparable with the most popular photoresist PMMA, the most well-known and widely used EBL resist. Both images were obtained under the acceleration voltage at 20 keV with the dose value of  $120 \mu\text{C}/\text{cm}^2$ , as shown in Fig. S5. From these images, we could believe that our PMAG resist is able to realize the spatial resolution of PMMA.

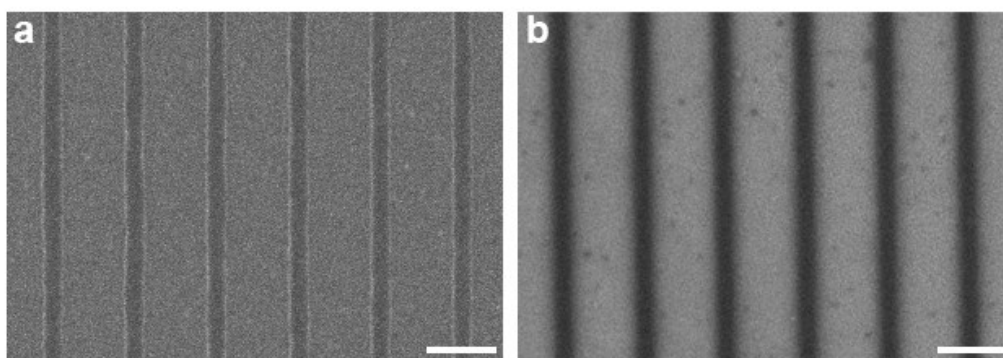


**Figure S5** | The spatial resolution comparison between PMMA and PMAG. (a, PMMA b, PMAG) The scale bars are 100 nm.

### One step formation of the 3D structure.

The PMAG resist could bear the ultra high dose factor to get some 3D structure arrays, shown in Fig. S6, like the volcano. As mentioned in the main text, both the crosslinking and the carbonization could take place during the electron beam exposure. Under the low exposure dose factor, the crosslinking came into prominence. As the dose factor increases, the carbonization degree could increase correspondingly, and we found that the exposed area was lit up by 405 nm laser. However, when the dose increased more, what will happen? Here we increased the exposed dose factor to an extremely high level of 1000. The 4×4 dot array was written under 20 keV acceleration voltage, 1000×120  $\mu\text{C}/\text{cm}^2$  dose value. As shown in Fig. S6, an array of volcano was obtained under this exposure condition. By zooming in the Fig. S6a, The shape of the volcano as presented in Fig. S6b indicates a clear trace of the electron beam scattering path. First, the PMAG exposure started from the volcano center as a dot. With the electron beam dose continuous injection, the surrounding area got more electron beam radiated from the center dot, and more PMAG crosslinked. Since the center dot was continuously exposed with electron beam, the carbonization degree in the center increased more and more, so we can see the central bulge, which could be clearly shown in the side view in Fig. S6c.

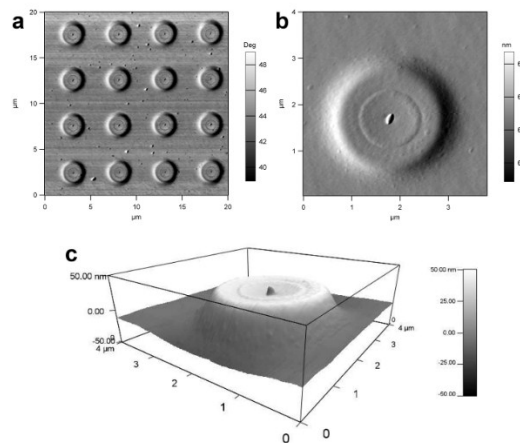


**Figure S6** | The volcano shape of PMAG.

## The EDAX measurement.

To understanding the difference in low dose and high dose treatment, the EDAX was used to detect the element distribution changing. Since the EDAX measurement itself is exposed under electron beam, here we just compare the carbon content at the same spot under different integration time. Under single time integration, the carbon content is around 47.6% and the oxygen content is around 23.1%. Under double times integration, the carbon content is 55.6%, and the oxygen content is 15.3%. Obviously, the carbon content increased by long time exposure; while the oxygen content decreased. This result was coordinated with the former reports that the volatile groups as  $\text{CO}_2$ ,  $\text{H}_2$ , and  $\text{CH}_3\text{O}$  would disappear via the electron beam treatment.<sup>[S3]</sup> This gave an additional evidence for the carbon quantum dots formation under the electron beam exposure.

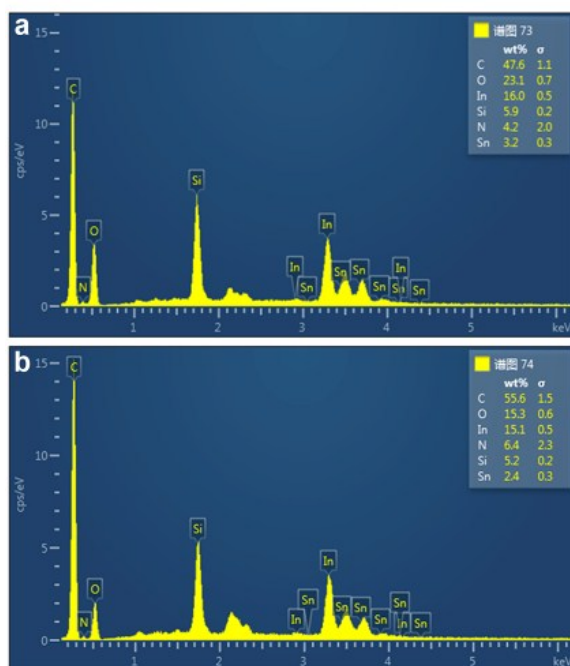


**Figure S7** | The EDAX analysis of the elements distribution of the local spot before (a) and after (b) electron beam treatment.

### The carbon quantum dots formation

In the main text, the histogram of the fluorescence intensity vs. the exposure dose factors was detected to find that the fluorescence intensity increased with dose and reached a stable value once the dose factor beyond 50, which is directly related with CQDs formation. Once the carbon cluster formed on the glycopolymer by the electron beam irradiation, the local modulation will change. By the phase model of the AFM, this local modulus change in the electron beam center could be detected easily. Figure S8 was a serial of the FFT images obtained by Fourier analysis of the 1  $\mu\text{m}$  scope. The dose factors in sequence from left to right were 1, 3, 5, 10, 15, 20, 50, 100 and 200. With the dose factor increasing, the carbonization degree increased correspondingly, so the carbon center could become clearer, as shown in the FFT analysis.

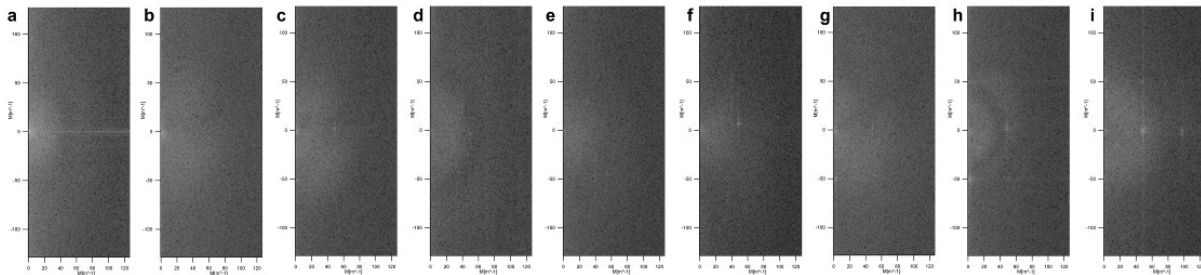


**Figure S8** | FFT of the phase image by AFM under different dose factors treatment.

(a-i: 1, 3, 5, 10, 15, 20, 50, 100, 200)

More than the precise tuning of the fluorescence intensity, the CQDs organization or ordering was another important issue in the related area application. In the main text, we demonstrated that the center dots distance was strictly controlled by the step setting in the exposure procedure. Here the 2D placement of the CQDs in array was shown in Fig. S9. Similar to the pattern in Fig.

3b', 2D array of 1  $\mu\text{m}$  squares was formed by different CQDs gaps. The step setting was tuned to be 20 nm, 40 nm, 60 nm and 100 nm in the exposure formulas. Hence under the FFT transition of these phase images, we could find that the periods change obviously and perfectly match the step setting (Fig. S9).

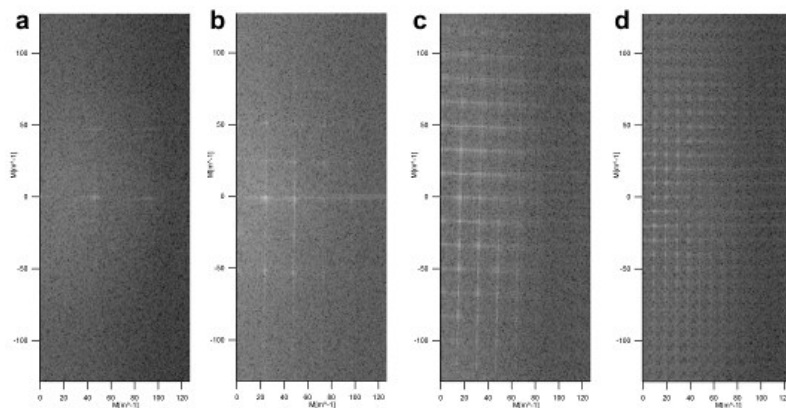


**Figure S9** | FFT of the phase image by AFM under different step treatment. (a-d: 20, 40, 60, 100 nm)

**The surface energy analysis of the PMAG film before and after electron beam treatment.**

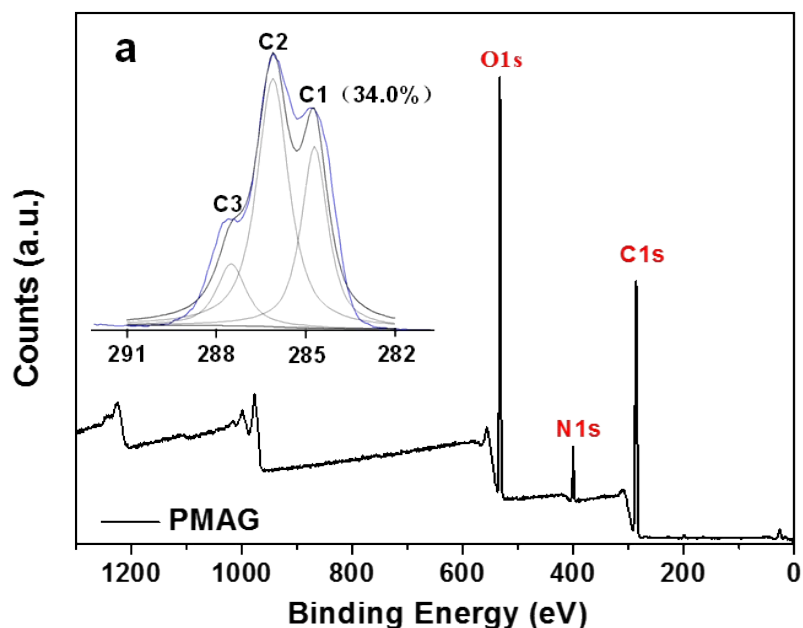
The bands in the range of  $1000\text{ cm}^{-1} \sim 1300\text{ cm}^{-1}$  in the blue box in Fig. 3d imply the C-OH stretching and OH bending vibration, and the coexistence of residual hydroxy groups could remain the hydrophilicity, but its amount decreased after electron beam treated. Hence the contact angle measurement was carried out. In Fig. S10, these two water drops were on the unexposed PMAG and exposed PMAG surfaces. The water contact angle on unexposed PMAG is  $12^\circ$ , and that on exposed PMAG is  $38^\circ$ . We could easily find that the surface hydrophilicity was worse after the electron beam treatment, which agree with the FT-IR result.



**Figure S10** | The contact angle of PMAG(a) and PMAG after electron beam treatment(b).

### The XPS measurement.

Figure S11 shows the XPS survey spectra of PMAG films before and after electron beam treatment without water development. The chemical compositions of these surfaces are summarized in Table S1. The PMAG after electron beam treatment shows a substantial increase in the C concentration, and decrease in the O concentrations compared with PMAG film. Furthermore, as shown in the inset of Fig. S11a&b, the percentage of the C2 peak (286.1 eV, -C-OH) decreased obviously, while C1 peak (284.7 eV) assigned to carbon atoms in -C=C- [S4] increased obviously from 34.0% to 49.3%. The XPS results are in consistent with the data from IR and Raman (Fig. 3), which indicate the aromatization of sugar in PMAG and the formation CQDs after electron beam treatment.



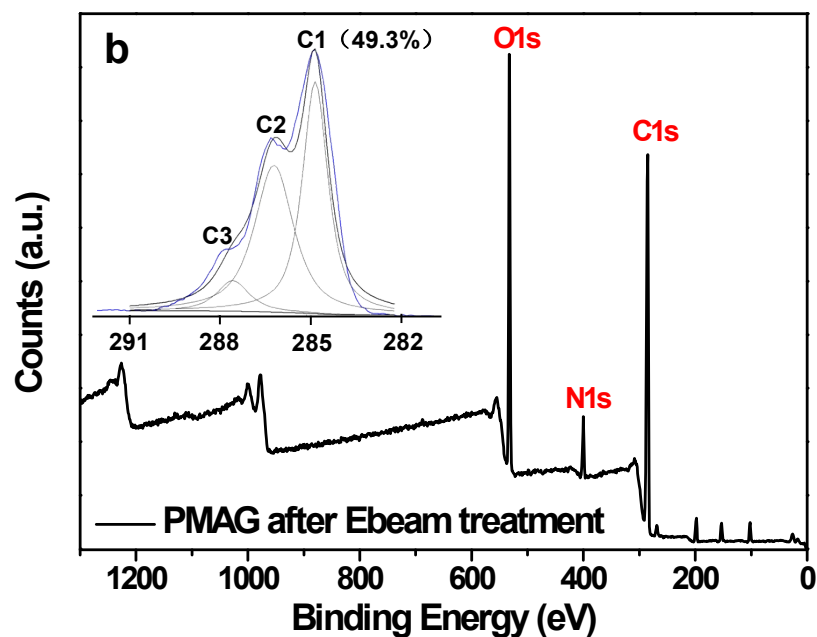


Figure S11 | XPS survey spectra of the PMAG before (a) and after (b) electron beam treatment. The high-resolution spectra of the C1s regions are shown in the inset.

**Table S1** | XPS analysis results for PMAG before and after electron beam treatment

XPS atomic concentration (%)			
Sample	C1s	O1s	N1s
PMAG	40.5	54.5	5.0
PMAG after electron beam treatment	47.8	46	6.2

### The effect of polymer structure by comparing polymers with different backbone and side chain

The polymer PMAG we synthesized has a backbone similar to PMMA and glucose side chain. We believe that both the PMMA backbone and the glucose side chain are necessary for realizing

the in-situ formation of carbon cluster and precise location control. Control experiments were carried out by the comparison of luminescent intensity of two other polymers with PMAG. We used poly(vinyl alcohol) (PVA, Mw = 31000) possessing the same backbone with PMMA without glucose in the side chain and dextran (Mw = 10000) bearing glucose units but has a different backbone to PMAG as resists. The three polymer were mixed with water to obtain 3% aqueous solution and was spin-coated on ITO glass. The results were shown in Fig. S12. The fluorescent images were obtained by the confocal system under the same pinhole and laser intensity. Figure S12a-c are the samples of the PVA, PMAG and dextran. We could see that without the glucose side chains, the carbon clusters were harder to be formed, so under the same expose dose factor ( $100 \times 120 \mu\text{C}/\text{cm}^2$ ), the luminescent images were darker, compared to the PMAG. Hence, we could demonstrate the combination of a glucose-containing side chain and a similar backbone to the commercial electron beam resist PMMA was necessary for the fine image and the carbon dots formation.

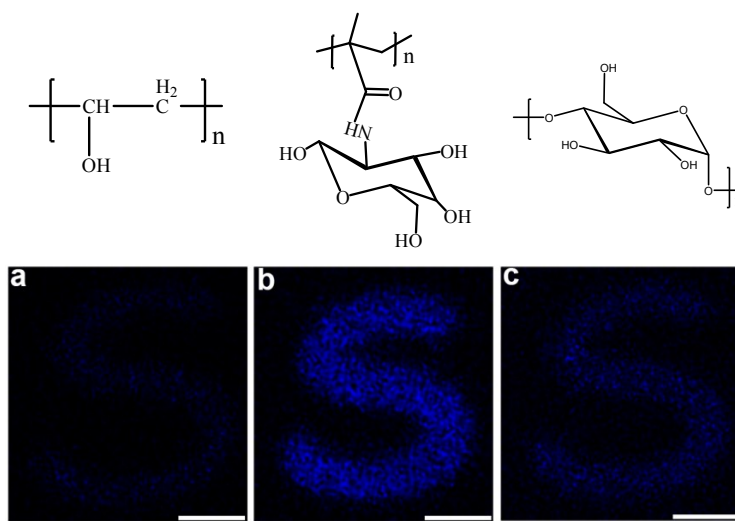


**Figure S12** | The confocal images of the PVA, PMAG and dextran samples. **a**, PVA, **b**, PMAG, **c**, Dextran. Scale bar is 20  $\mu\text{m}$ .

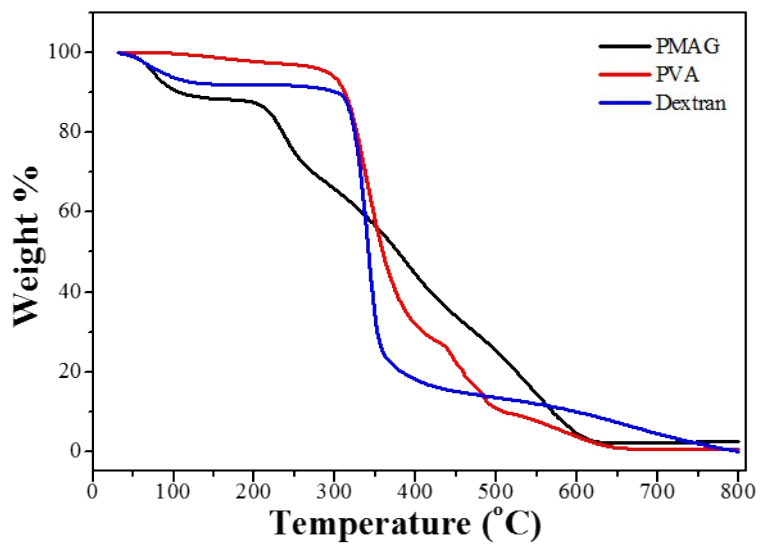


**Figure S13** | The thermal gravimetric analysis (TGA) of the PVA, PMAG and Dextran samples.

**The fluorescence properties of the PMAG**

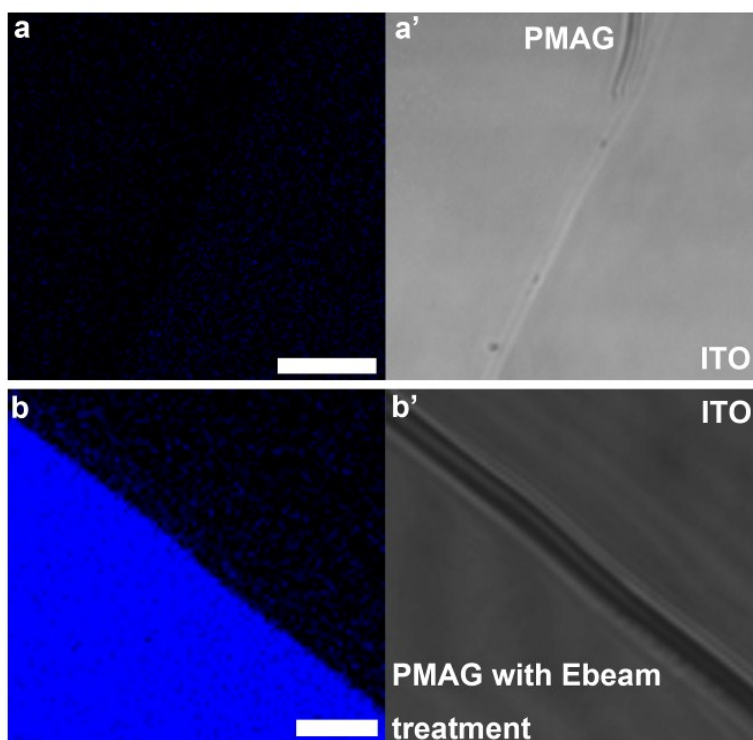


**Figure S14** | **a**, The confocal (a) and microscopic (a') images of PMAG, the confocal (b) and microscopic (b') images of the electron beam treated PMAG film. The scale bar in **a** is 10  $\mu\text{m}$ , and that in **b** is 5  $\mu\text{m}$ .

In order to verify the PMAG fluorescence happened after the electron beam exposure, the confocal characterizations of the PMAG film before and after electron beam exposure were shown in Fig. S14. Figure S14a-a' are the PMAG film before the electron beam exposure. Figure S14a was the confocal image and Fig. S14a' was the optical one. Results show that the unexposed PMAG film could not be lit up by 405 nm laser. Figure S14b-b' are the PMAG film after the electron beam exposure, demonstrating that the exposed PMAG film could be lit up by 405 nm laser as shown in Fig. S14b.

The fluorescent images with fine structure are shown in Fig. S15. Corresponding emissions of the three patterns (the square, line and lattice arrays) are clearly observed in Fig. S15a'-c'.

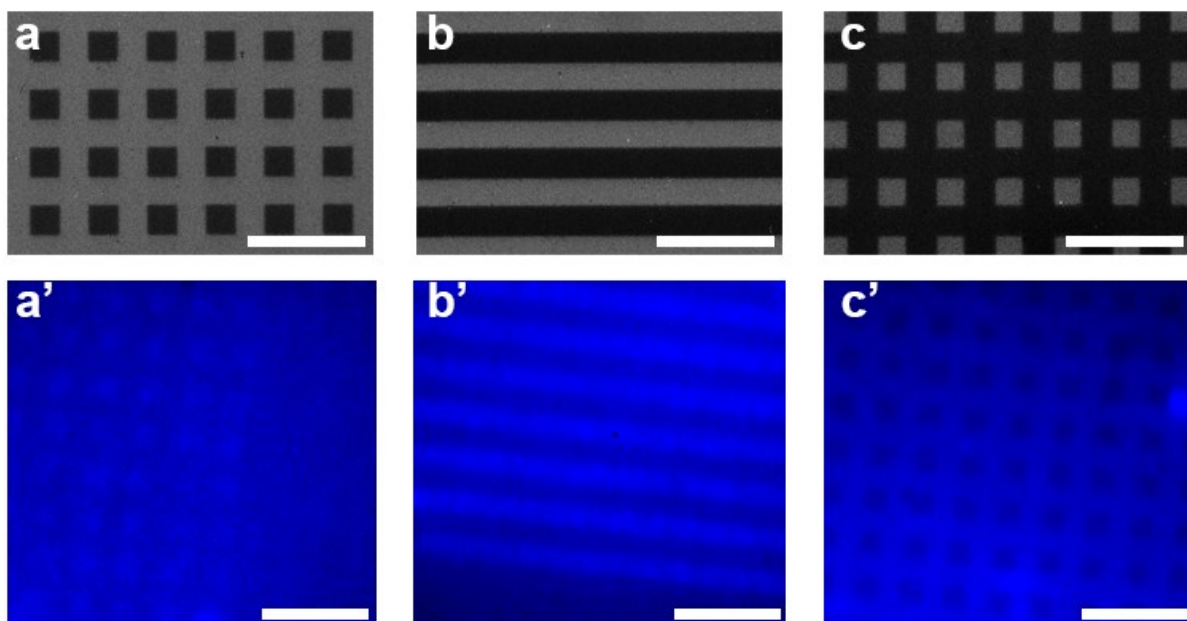


**Figure S15** | The fluorescent images of different structure (a-c, SEM images; a'-c', Fluorescent images of super resolution microscope) The scale bars in the images are 10  $\mu\text{m}$ .

The fluorescence intensity could be varied by importing different counts of the CQDs, as shown in Fig. S16. The golden plate was employed as a target object. Figure S16a-c are SEM images of the CQDs morphology, and Fig. S16a'-c' are the corresponding fluorescent images. For the bare golden plate which could not be lit up by 405 nm laser, we find the dark spot in the center of Fig. S16a'. Figure S16b is the golden plate with one circle of the CQDs, and a bright fluorescent circle outside of the dark center could be found in Fig. S16b'. For the golden plate with 3 concentric circles of CQDs, they could be lit up by 405 nm laser and presents stronger fluorescence as shown in Fig. S16c'. Hence, by placing different amount of the CQDs in different morphologies could result in different performance in the fluorescent images in nanoscale, demonstrating the importance of the precise location and amount of the CQDs in nano-structural materials.

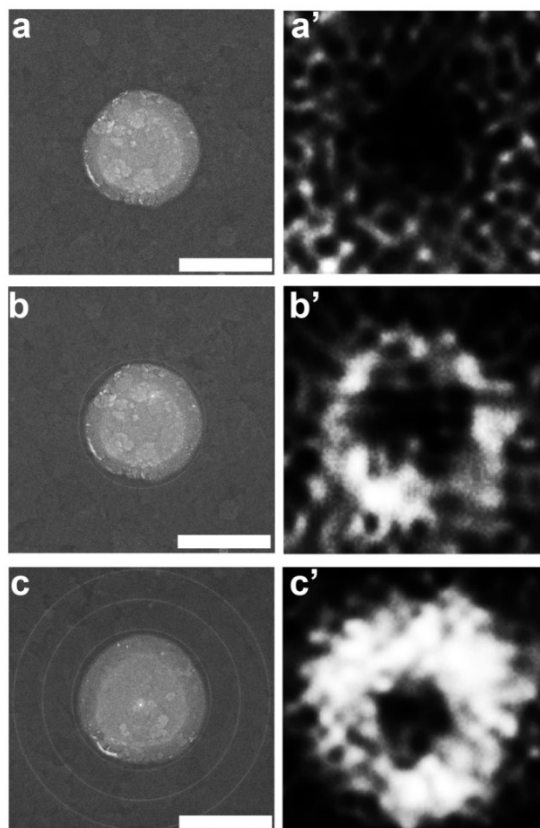


**Figure S16** | The fluorescent images of different structure. (**a-c**, SEM images, **a' -c'**, Fluorescent images under super resolution microscope) The Scale bars in the images are 300 nm.

- [S1] Zhang, Z., Zhu, X., Zhu, J., Cheng, Z. & Zhu, S. *J. Polym. Sci., Part A: Polym. Chem.* **44**, 3343 (2006).
- [S2] Ting, S. R. S., Min, E. H., Zetterlund, P. B. & Stenzel, M. H. *Macromolecules* **43**, 5211 (2010).
- [S3] Chen, W., Yu, Y., Zheng, X., Qin, S., Wang, F., Fang, J., Wang, G., Wang, C., Wang, L., Peng, G., Zhang, X. *Scientific Reports* **5**, 12198 (2015).
- [S4] Shen W., Li Z. & Liu Y. Surface Chemical Functional Groups Modification of Porous Carbon. *Rec. Pat. Chem. Eng.* **1**, 27-40 (2008).